Interaction of Artepillin C with model membranes

Interaction of Artepillin C with model membranes

Wallance Moreira Pazin[a,d], Danilo da Silva Olivier[a,d], Neus Vilanova[b], Ana Paula Ramos[a], Ilja Karina Voets[b,d], Ademilson Espencer Egea Soares[c] and Amando Siuiti Ito[a,*]

[a] Departments of Physics & Chemistry, Faculty of Philosophy, Sciences and Letters of Ribeirão Preto, University of São Paulo, Brazil

[b] Macromolecular and Organic Chemistry, Physical Chemistry & Institute for Complex Molecular Systems, Eindhoven University of Technology, the Netherlands

[c] Ribeirão Preto Medical School, University of São Paulo, Brazil

[d] Dutch Polymer Institute (DPI), PO Box 902, 5600 AX Eindhoven, the Netherlands

* Corresponding author:

E-mail address: amandosi@ffclrp.usp.br

Av. Bandeirantes, 3900,

14040-901, Ribeirão Preto, Brazil

Tel.: +55 16 3315 3809

Acknowledgements

We thank Dr. Georg Pabst for help with the GAP software, Dr. Galina Borissevitch for useful discussion on the monolayer experiments and Cynthia Maria de Campos Prado Manso for helping to revise the English language. The research was supported by the Brazilian agencies CAPES, CNPq (process numbers 232302/2014-6 and 304981/2012-5), and FAPESP (process number 2014/26895). This research is part of the research program of the Dutch Polymer Institute (DPI), projects #772a and #772ap.

Abstract

Green propolis, a mixture of beeswax and resinous compounds processed by *Apis mellifera*, displays several pharmacological properties. Artepillin C, the major compound in green propolis, consists of two prenylated groups bound to a phenyl group. Several studies have focused on the therapeutic effects of Artepillin C, but there is no evidence that it interacts with amphiphilic aggregates to mimic cell membranes. We have experimentally and computationally examined the interaction between Artepillin C and model membranes composed of dimyristoylphosphatidylcholine (DMPC) because phosphatidylcholine (PC) is one of the most abundant phospholipids in eukaryotic cell membranes. PC is located in both outer and inner leaflets and has been used as a simplified membrane model and a non-specific target to study the action of amphiphilic molecules with therapeutic effects. Experimental results indicated that Artepillin C adsorbed onto the DMPC monolayers. Its presence in the lipid suspension pointed to increased tendency toward unilamellar vesicles and to decreased bilayer thickness. Artepillin C caused point defect in the lipid structure, which eliminated the ripple phase and the pre-transition in the thermotropic chain melting. According to molecular dynamics (MD) simulations, (i) Artepillin C aggregated in the aqueous phase before it entered the bilayer; (ii) Artepillin C was oriented along the direction normal to the surface; (iii) the negatively charged group on Artepillin C accommodated in the polar region of the membrane; and (iv) thinner regions emerged around the Artepillin C molecules. These results helped to understand the molecular mechanisms underlying the biological action of propolis.

Keywords: DMPC; Model membranes; Artepillin C; Green Propolis; Langmuir monolayer.

Introduction

Propolis results from a mixture of beeswax and resinous compounds that bees selectively collect from the vegetation. This mixture has long been used as an antibacterial, antifungal, and antioxidant agent in traditional medicine (Bastos, Simone, Jorge, Soares, & Spivak, 2008; Lotfy, 2006; Sawaya, 2009). The biological activity of propolis is related to the presence of natural substances such as bioactive secondary metabolites from plants. Therefore, the final composition of propolis strongly depends on the bee species and on the region the bees inhabit (Alhassan, Abdullahi, Uba, & Umar, 2014; Kumazawa, Hamasaka, & Nakayama, 2004; Yong K. Park, Severino M. Alencar, 2002). Phenolic acids, flavonoids, and terpenes are the commonest substances collected by several species of bees worldwide (Arslan, Silici, & Percin, 2012; Bonvehí & Gutiérrez, 2012; Gregoris & Stevanato, 2010; Hamasaka, Kumazawa, Fujimoto, & Nakayama, 2004; Laskar, Sk, Roy, & Begum, 2010; Righi, Negri, & Salatino, 2013). These substances protect beehives against intruders and ensure their antisepsis.

Green propolis from the species *Apis mellifera* has a broad spectrum of biological and pharmacological properties. The Brazilian green propolis is famous for its antitumor potential, especially due to the presence of Artepillin C (3,5-diprenyl-4-hydroxycinnamic acid), which is the major constituent among all the compounds identified in this propolis (Kimoto et al., 1998). Artepillin C also displays anti-inflammatory and anti-oxidant properties (Paulino et al., 2008; Shimizu, Ashida, Matsuura, & Kanazawa, 2004), and it is an important lead in the search for new drugs even though its mechanism of action is not well established yet. This molecule belongs to the group of cinnamic acid derivatives. It has low molecular weight (300.39 $g \cdot mol^{-1}$) and bears two prenylated groups bound to a phenyl

group (Figure 1). This particular structure enhances the hydrophobicity of Artepillin C and probably favors its interaction with amphiphilic aggregates such as cell membranes (Alhassan et al., 2014), which may be the step that elicits its biological action. However, the interaction between Artepillin C and cell membranes or cell membrane models is not well understood.

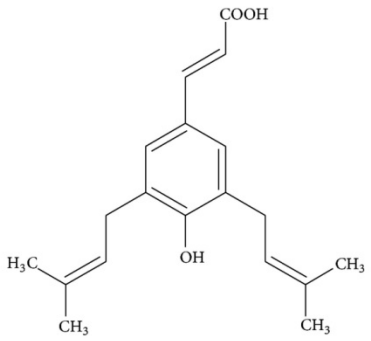

Figure 1. Molecular structure of Artepillin C

In this study, we have examined the interaction of Artepillin C with cell membrane models such as vesicles and Langmuir monolayers consisting of dimyristoylphosphatidylcholine (DMPC). We decided to use DMPC because it is one of the most abundant phospholipids in eukaryotic cell membranes and is located in both outer and inner leaflets. Phosphatidylcholine (PC) has been extensively explored as a model for the basic structure of cell membranes and has been employed as a non-specific target for the action of amphiphilic molecules with therapeutic effects (Barioni, Ramos, Zaniquelli, Acuña, & Ito, 2015; Fa et al., 2006; Ota, Abramovič, Abram, & Poklar Ulrih, 2011; Suwalsky et al., 2015; Tovani et al., 2013; Wesołowska, Gąsiorowska, Petrus, Czarnik-Matusewicz, & Michalak, 2014). To probe the thermotropic lipid phase transition, we have

resorted to differential scanning calorimetry (DSC). Small angle X-ray scattering (SAXS) helped us to investigate alterations in the structural properties of the lipid bilayers. The adsorption of Artepillin C at the water/lipid interface was monitored by z-potential measurements and surface pressure vs surface area isotherms. In addition, molecular dynamics (MD) simulations helped us to evaluate how Artepillin C accessed the lipid bilayer, to identify its specific location in the membrane, and to verify structural changes in the bilayer after the interaction.

Material and Methods

Chemicals

1,2-Dimyristoyl-*sn*-glycero-3-phosphocholine (DMPC) was purchased from Avanti Polar Lipids (Alabaster, AL, USA) as powder. Artepillin C (3,5-diprenyl-4-hydroxycinnamic acid), isolated and purified from Brazilian green propolis, was purchased from Wako, Japan. All the reagents were used without further purification. Lipid suspensions were prepared by using dust-free Milli-Q water (18.2 MΩ·cm).

Preparation of vesicles

Large unilamellar vesicles (LUVs) and multilamellar vesicles (MLVs) were prepared from stock solutions of DMPC lipids in chloroform at 40 $mmol \cdot L^{-1}$. Vesicles containing Artepillin C were obtained by mixing controlled amounts of a 20 $mmol \cdot L^{-1}$ stock solution of the compound in methanol (MeOH) with the lipid solution in chloroform. Dry films emerged by evaporating the solvent under a N_2 flow and eliminating the remaining traces of organic solvent under reduced pressure for at least 1 h. The MLVs were prepared by adding Milli-Q water onto the films and vortexing them at 30 °C for 2 min, above the lipid phase transition temperature. Subsequent extrusion afforded the LUVs, as described elsewhere

[22,23]. The MLV suspension was passed through a polycarbonate membrane with pores measuring 0.1 µm (Whatman, Sigma Aldrich) at least 21 times. Previous work on dynamic light scattering (DLS) performed in our group had shown this procedure resulted in a sharp distribution of particles with diameter of 120 nm and a single population when the process occurred above the phase transition temperature. The turbidity of the preparation remained stable during the period the experiments were conducted.

Langmuir Monolayers

A 1 $mmol \cdot L^{-1}$ DMPC solution in chloroform was spread on a 216-cm^2 (length = 21.95 cm; width = 9.85 cm) Langmuir trough (Insight-Brazil). After evaporation of the organic solvent, the mobile barrier was moved at a constant rate of 0.041 $cm \cdot s^{-1}$, to form the lipid monolayer at the air/liquid interface. Either pure water or 1 $\mu mol \cdot L^{-1}$ Artepillin C aqueous solution was used as subphase. The surface vs surface area (π–A) isotherms were recorded at 25 °C, and the area expansion due to Artepillin C adsorption was calculated by subtracting the isotherm obtained in the absence of the compound from the isotherm obtained in the presence of the compound (Parra, Borissevitch, Borissevitch, & Ramos, 2015).

Zeta potential measurements

The electrophoretic mobility of DMPC unilamellar vesicles (1 mmol·L^{-1}) was measured in the absence and in the presence of Artepillin C (Artepillin C/DMPC molar ratio 2:100, 5:100, 7.5:100, 15:100, and 20:100) to compute the z-potential by means of the Smoluchowski equation (Shaw, 1992):

$$\zeta = \frac{\eta \mu}{\varepsilon}, \qquad (1)$$

where η is the viscosity of the solvent, μ is the electrophoretic mobility, and ε is its dielectric constant. Samples containing Artepillin C were prepared by adding aliquots of a 10 mmol·L^{-1} solution of this compound in MeOH to the extruded suspension. The measurements were performed on a Nano Zetasizer ZS90 (Malvern Instruments, Worcestershire, U.K), which uses a wide-angle (178°) laser Doppler velocimetry, at 30 °C. The samples were placed in dedicated plastic cuvettes (DTS1060 cells) equipped with gold electrodes (Malvern Instruments).

Small angle X-ray scattering (SAXS)

SAXS measurements were performed on a SAXSLAB GANESHA 300 XL SAXS system equipped with a GeniX 3D Cu Ultra Low Divergence micro focus sealed tube source that produced X-rays with a wavelength of λ = 1.54 Å. A sample-to-detector distance of 713 mm was used to access a q-range of $0.15 \leq q \leq 4.47$ nm^{-1} with $q = 4\pi/\lambda(\sin\theta/2)$, where 2θ was the angle between the incident X-ray beam and the detector measuring the scattered intensity. Extruded lipid suspensions at 40 mmol·L^{-1} in the absence and in the presence of

10 mol% of Artepillin C were placed in 2-mm quartz capillaries (Hilgenberg, Germany). The sample temperature was kept at 30 °C with the aid of a Julabo temperature controller. The acquisition time of the SAXS data was 6 h for each sample, and the background signal (scattering of a capillary filled with water) was subtracted from the obtained profiles. The experimental SAXS diagrams were fitted by using the Global Analysis Program (GAP) version 1.3, provided by Dr. Georg Pabst of the Austrian Academy of Sciences – Graz. Herewith, we obtained the electron density of the polar head group, of the acyl chain regions of the lipid bilayers, and of the fraction of the resulting unilamellar vesicles (Pabst et al., 2003; Pabst, Rappolt, Amenitsch, & Laggner, 2000) by using the function:

$$I(q) = (1 - N_{UV})\frac{S(q)|F(q)|^2}{q^2} + N_{UV}\frac{|F(q)|^2}{q^2}, \qquad (2)$$

where N_{UV} is the fraction number of positionally non-correlated particles (i.e., unilamellar vesicles), *S(q)* is the structure factor (inter-particle interaction), and *F(q)* is the form factor, which gives the electron density profile. From the parameters that describe the head group regions, it was possible to calculate the thickness of the membrane (d_B) through equation (Pabst et al., 2008):

$$d_B = 2(z_H + 2\sigma_H), \qquad (3)$$

where z_H is the headgroup position measured from the center of the bilayer, and σ_H is the width of the Gaussian of the electron-dense distribution over the headgroup region.

Differential scanning calorimetry (DSC)

Calorimetric experiments were carried out on a VPN-DSC from Microcal. The capillary degassed samples of MLVs (10 $mmol \cdot L^{-1}$) were placed in the analyzer in the absence and in the presence of 1, 5, and 10 mol% of Artepillin C. The scan rate was 0.5 $°C.min^{-1}$ throughout the experiments. The Microcal Origin software, provided by Microcal, allowed us to subtract the baseline and analyze the data. Each sample was scanned at least seven times. The samples were prepared in triplicate.

Molecular Dynamics Simulations (MD)

Molecular Dynamics (MD) simulations were performed with the NAMD 2.10 (Phillips et al., 2005)software on a fully hydrated DMPC bilayer in the presence of different concentrations of Artepillin C molecules. The DMPC bilayer containing 64 lipids per leaflet was previously equilibrated until it reached the experimentally reported values of area per lipid and thickness (Kučerka, Nieh, & Katsaras, 2011). The parameters for Artepillin C were obtained by using the webserver CGenFF (Vanommeslaeghe et al., 2010; W. Yu, He, Vanommeslaeghe, & MacKerell, 2012). Two different systems were built by employing packmol (Martínez, Andrade, Birgin, & Martínez, 2009) and different Artepillin C/lipid molecular ratios, namely 5:128 and 10:128. The low concentration system contained 34,411 atoms with five sodium ions, whereas the high concentration system had 34,626 atoms with 10 sodium ions. In both cases, the simulation started with Artepillin C molecules placed in the bulk. To eliminate bad contacts between the atoms, we initially minimized the starting structures and equilibrated the system for 2 ns. Afterwards, we

performed a 500-ns simulation for both systems. For these simulations, the CHARMM C36 (Klauda et al., 2010) force field was applied. Moreover, the NPT ensemble was employed at 313 K and pressure of 1 bar. To control the temperature and pressure, we used Langevin Dynamics and Nosé-Hoover Langevin, respectively. The long-range electrostatic interactions were estimated by using the Particle-Mesh-Ewald summation method with a cutoff of 1.2 nm and switch distance of 1.0 nm. The results of the simulations were analyzed with LOOS v2.2.5 (Romo, T.D., Grossfield, 2009), and figures were prepared by using VMD (Humphrey, Dalke, & Schulten, 1996).

Results and Discussion

DMPC monolayers: π–A isotherms

First, a DMPC *π–A* isotherm was obtained with a pure water subphase (Figure 2A - black line). The monolayer was compressed from 0 up to its collapse, which occurred at a surface pressure of approximately 47 mN/m. At 25 °C, the isotherm evidenced a liquid-expanded phase over all the compression of the monolayer, as expected for this phospholipid (Gaboriaud, Volinsky, Berman, & Jelinek, 2005; Gradella Villalva et al., 2016; Ramos, Pavani, Iamamoto, & Zaniquelli, 2010). The isotherm expanded upon addition of Artepillin C to the subphase (Figure 2A, red line). With 1 $\mu mol \cdot L^{-1}$ Artepillin C, the collapse happened at a surface pressure of 50 mN/m, which represented a slight increase of 3 $mN \cdot m^{-1}$ as compared to the pure water subphase. This increase indicated larger barrier against compression.

Artepillin C expanded the area of the DMPC monolayer as revealed by the difference between the molecular lipid areas of the isotherms measured in the pure water subphase and in the presence of the compound. Increased surface pressure decreased the expanded area (Figure 2B), which reached a constant value close to 2 $Å^2$ at surface pressures above 30 $mN \cdot m^{-1}$. This corresponded to an area expansion of around 4% in the

DMPC monolayer at its maximum packing, which was caused by insertion of Artepillin C molecules.

A surface effect promoted by the deprotonated form of Artepillin C, which displays a negative charge on the oxygen located in the carboxylic group of the cinnamic acid with pK_a value of 4.4, may have increased the surface pressure required to collapse the monolayer and expanded the observed area (J. Q. Yu & Matsui, 1997). This should expand the monolayer and demand higher energy to compensate for the electrostatic repulsion between the charges of the Artepillin C molecules in the monolayer. The presence of negative charges in the monolayer and the corresponding changes in the electric surface potential could be related to the zeta potential experiments, as follows.

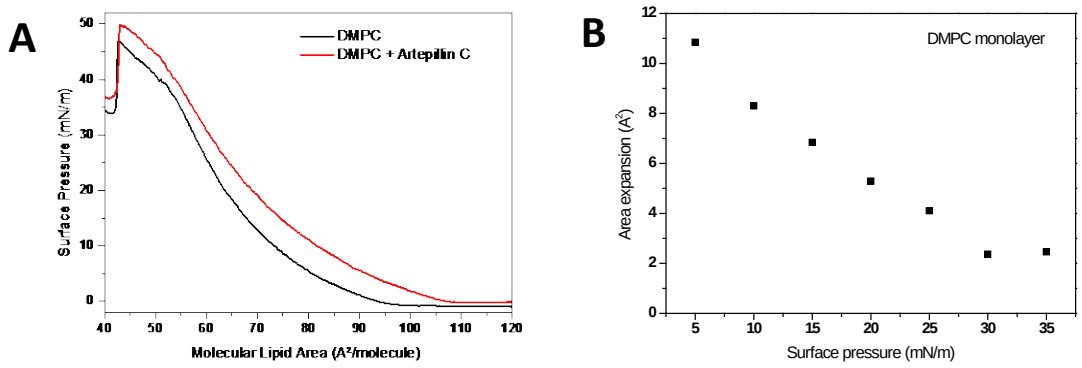

Figure 2. A) Isotherms recorded for the DMPC monolayer in the absence (black line) and in the presence (red line) of Artepillin C, at 25 °C. B) Area expansion obtained from the difference between the areas per molecule of the phospholipid isotherms, obtained in the pure water subphase and recorded in the presence of Artepillin C molecules, as a function of the surface pressure

Zeta potential

Zeta potential measurements evidenced the charge effects of Artepillin C at the polar head group region of the lipid unilamellar vesicles. Figure 3 shows the changes in the z-potential of DMPC vesicles as a function of the amount of Artepillin C added to the system. Despite the electrical neutrality of pure DMPC, a negative potential of – 4.2 mV was detected. This potential basically originated from the negative charge on the phosphate group of DMPC molecules. The z-potential decreased slightly when 2.5 mol% Artepillin C was added to the DMPC vesicles. Addition of 5 and 20 mol% Artepillin significantly reduced the surface potential to values around –10.0 and -16.7 mV, respectively. These changes indicated that Artepillin C inserted into the bilayer and modified the negative charge density on the vesicle surface. This could be caused by the O^- located in the carboxylic group of the cinnamic acid, which affected the zwitterionic polar head region of the lipid vesicle. The decrease in the vesicle surface potential could result from electrostatic contribution to the π-A results: a higher surface pressure was necessary to collapse the expanded monolayer containing the deprotonated structure of Artepillin C.

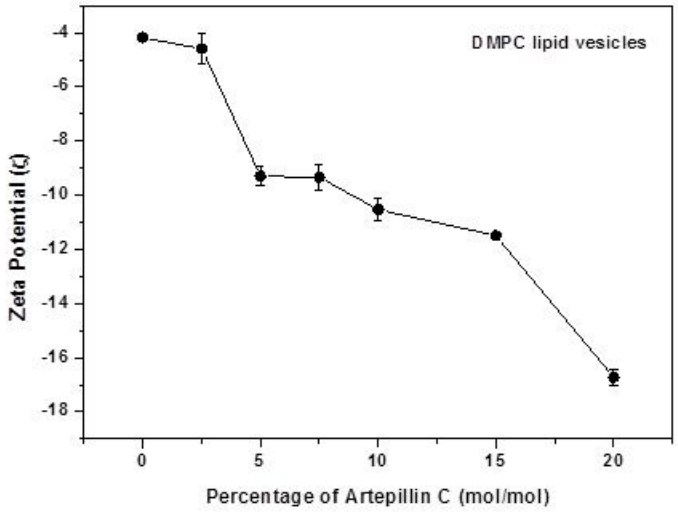

328

329 **Figure. 3 Zeta potential of DMPC vesicles in the absence and in the presence of Artepillin C,**
330 **obtained at 30 °C**

331

332 **Small Angle X-ray Scattering (SAXS)**

333 Structural changes in DMPC vesicles induced by Artepillin C were examined by small
334 angle X-ray scattering experiments. The results were analyzed in terms of the electron
335 density distribution of the hydrophobic and hydrophilic regions of the bilayers. The SAXS
336 pattern of DMPC extruded vesicles without Artepillin C displayed a broad quasi-Bragg
337 peak around 0.1 $Å^{-1}$ and a shoulder around 0.2 $Å^{-1}$ (Figure 4A), which indicated the
338 presence of multilamellar vesicles despite the extrusion procedure (Ristori et al., 2009).
339 From the fit of the curves to the experimental data given by equation 2, and by using the
340 values obtained for d_B, calculated as shown in equation 3, it was possible to obtain the
341 structural parameters presented in Table 1. By far the most prominent difference was the

increased percentage of unilamellar vesicles (N_{UV}) upon insertion of Artepillin C: the percentages of DMPC unilamellar vesicles (LUVs) in the absence and in the presence of Artepillin C were 64% and 96%, respectively. Artepillin C presumably accommodated in the polar head group region. Because it is negatively charged, Artepillin C should generate an inter-bilayer electrostatic repulsion, to form LUVs spontaneously, as reported elsewhere for other charged compounds (Ristori et al., 2009). This was consistent with the results from the z-potential measurements. The other structural parameters (Table 1) revealed that the presence of Artepillin C slightly thinned the lipid bilayer, by around 2%.

The SAXS data evidenced that Artepillin C affected LUVs in almost the same way as the procedures conducted to obtain unilamellar vesicles; for instance, addition of a small percentage of negatively charged lipids to the suspension resulted in inter-bilayer electrostatic repulsion. Further experiments with non-extruded lipid suspension (data not shown) corroborated this feature: the diagram obtained for the sample without Artepillin C was typical of multilamellar vesicles. However, addition of the bioactive compound to the non-extruded suspension culminated in a profile that was characteristic of unilamellar vesicles. Moreover, fitting of both diagrams provided Nuv values that corresponded to the amount of unilamellar vesicles in the non-extruded suspension and indicated the presence of around 29% and 99% of LUVs for the pure and for the Artepillin C-containing suspensions, respectively.

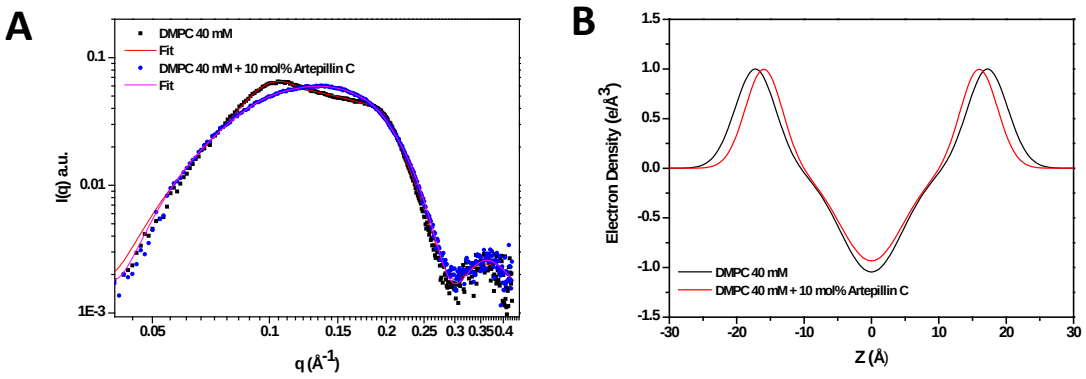

361

362 **Figure. 4 SAXS diagrams (A) and electron density (B) profiles of extruded DMPC lipid**
363 **vesicles in the absence and presence of 10 mol% of Artepillin C, obtained at 30 °C. Electron**
364 **density profiles were obtained by fitting the SAXS curves with the aid of the GAP software**
365 **(version 1.3)**

366

367 **Table 1. Structural parameters obtained by fitting the SAXS profiles of DMPC extruded**
368 **vesicles in the absence and in the presence of 10 mol% Artepillin C. Z_H: headgroup position;**
369 **σ_H: width of the electron density distribution over the headgroup region, N_{UV}: percentage of**
370 **unilamellar vesicles; d_B: thickness of the lipid bilayer. Estimated deviations are 1%**

Extruded vesicles	Z_H (Å)	σ_H (Å)	N_{UV} (%)	d_B (Å)
DMPC 40 mM	17.2	3.0	64	46.4
DMPC 40 mM + 10 mol% Artepillin C	16.9	2.9	97	45.4

371

372 **Differential Scanning Calorimetry (DSC)**

An increase in temperature causes DMPC multilamellar vesicles to undergo transition from a gel ($L_{\beta'}$) to a fluid phase (L_{α}). The data obtained here agreed with the results of Prenner et al. (Prenner, Lewis, Kondejewski, Hodges, & McElhaney, 1999) and showed that the transition gave rise to a sharp peak at 23.9 °C (T_M) in the thermogram, which was associated with an enthalpy value of 7.2 kcal/mol (Figure 5). Additionally, a pre-transition peak (T_P) emerged at 14.3 °C with a variation in enthalpy of 1.26 kcal/mol. This peak reflected the conformational change of the carbon chains from a lamellar gel phase to a ripple gel phase. Addition of 1 mol% of Artepillin C altered the cooperativity of the lipids in the vesicles. The main peak shifted and broadened slightly, which strongly modified the pre-transition peak and concomitantly increased and decreased the enthalpy of both endothermic processes, respectively (Table 2). The pre-transition peak shifted downward by -3.6 °C, which was accompanied by a reduction in ΔH_P from 1.26 to 0.68 kcal/mol (54%). These changes suggested that Artepillin C could be located near the lipid/water interface, thereby affecting the properties of the polar headgroup region, as already reported for other compounds (Basso, Rodrigues, Naal, & Costa-Filho, 2011; Gardikis, Hatziantoniou, Viras, Wagner, & Demetzos, 2006; Wesołowska et al., 2014). For higher Artepillin C concentrations of 5 and 10 mol%, the pre-transition peak completely disappeared, the main peak broadened and shifted to lower temperatures, and the associated enthalpy decreased, which indicated that the presence of the bioactive compound strongly impacted both transitions. Indeed, the fact that the addition of biomolecules changes the DMPC pre-transition temperature has already been reported. For instance, cholesterol decreases T_P, while other compounds such as gramicidin S, cannabinoids, sphingosine, various anesthetics, and ceramides completely abolish it (T Heimburg, 2000). As reported

before (Thomas Heimburg, 1998), the pre-transition in DMPC vesicles has half width in the range of 1 °C and is considerably less cooperative than the main transition, which has half width of 0.05 °C.

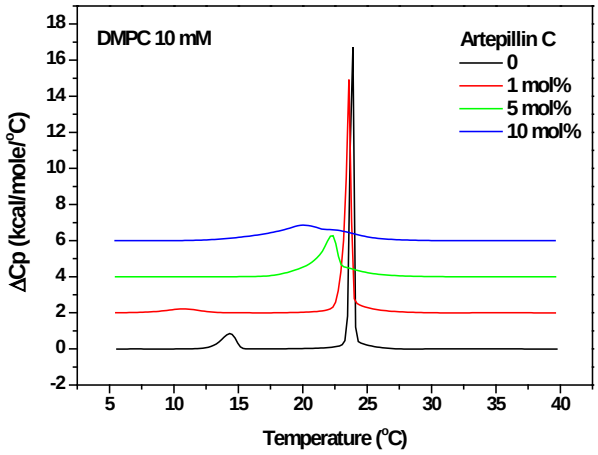

Figure 5. DSC thermograms of DMPC multilamellar vesicles, spanning from 5 to 40 °C

Table 2. Thermodynamic data obtained from DSC measurements of DMPC (control) and Artepillin C-inserted DMPC vesicles (1 , 5 and 10 mol%). T_P: pre-transition temperature; ΔH_P: pre-transition enthalpy change; T_M: main transition temperature; ΔH_M: main transition enthalpy change. Estimated deviations are 1%

DMPC 10 mM	T_p (° C)	ΔH_p (kcal/mol)	T_m (° C)	ΔH_m (kcal/mol)
Pure	14.3	1.26	23.9	7.2
1 mol%	10.7	0.68	23.6	8.3
5 mol%	-	-	22.3	5.7

10 mol%	-	-	20.1	5.7

Heimburg (2000) presented a model for the thermotropic phase transition in lipid vesicles that considered both the pre- and the main melting transitions as part of the lipid chain melting, associated with the formation of periodic ripples on the membrane surface. Within the model, the formation of membrane ripples, which consist of fluid lipid line defects, could be a consequence of the coexistence of gel and fluid lipid domains within an individual monolayer. Due to geometrical and topological constraints, such domains are forced to arrange periodically on the surface. Therefore, in the framework of this model, the pre- and main transitions are coupled, and an isolated monolayer should not form ripples.

According to the SAXS results, insertion of Artepillin C into DMPC vesicles forced the formation of unilamellar vesicles. Geometrical changes also occurred in the bilayer, as seen by the 2% decrease in the thickness of the bilayer and the concomitant extension of the surface. Hence, the structural arrangement of the DMPC vesicles in the presence of Artepillin C should modify their thermotropic behavior in such a way that the fluid lipid line defects would be avoided, thus preventing the formation of line defects that could originate the ripple phase and the pre-transition.

Molecular Dynamics Simulations (MD)

To clarify the interaction between Artepillin C and the DMPC lipid bilayer, we carried out atomistic molecular dynamics simulations. Two different Artepillin C/lipid molecular ratios, 5:128 and 10:128, were investigated. In the initial configuration, all the Artepillin C

molecules were placed in the bulk (Figure 6A), and the simulations were run for over 500 ns (Figures 6A to 6F). At the end of the simulation, the Artepillin C molecules were inside the lipid bilayer (Figure 6F). To evaluate the interaction between the compound and the bilayer in more detail, we counted the number of contacts between two Artepillin C molecules or between the compound and other components of the system. To this end, we created a shell in the target molecule (Artepillin C) and computed the number of atoms residing inside the shell to obtain the percentage of contacts between the target molecule and the second compound.

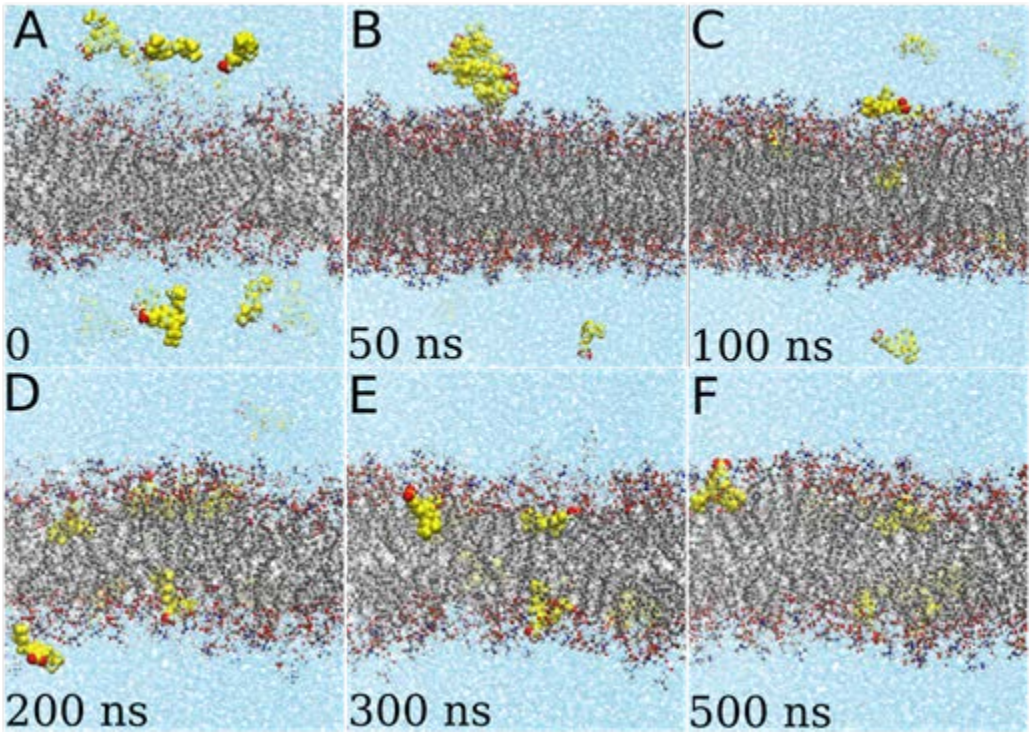

Figure. 6 Artepillin C interacting with a DMPC lipid bilayer: snapshots from MD simulations over 500 ns for the system containing 10 Artepillin C molecules and 128 DMPC lipids molecules. The lipid bilayer and the water molecules were replicated in the x-y plane. In addition, the snapshots corresponded to different x-y positions (at the same z) of the bilayer, which improved visualization of the Artepillin C position in the bilayer.

Figure 6B shows that Artepillin C aggregated in the bulk before reaching the lipid bilayer. The contact map (Figure 7A – top, green line) confirmed the presence of aggregates within the first 100 ns: 88% of the total average contact took place between Artepillin C molecules. Hydrophobic interactions of Artepillin C in water promoted such aggregation, subsequently favoring insertion of this molecule into the lipid phase of the membrane. The contacts between Artepillin C and DMPC or water (Figure 7A – bottom) revealed how the compound entered the bilayer: in the first 100 ns, Artepillin C molecules had some contact with water molecules (blue line), which surrounded the Artepillin C aggregates. However, Artepillin C had no contact with the DMPC bilayer (magenta line), then. From 100 to 300 ns, Artepillin C molecules started entering the membrane (snapshots C, D, and E in Figure 6), increasing the percentage of average contacts with DMPC lipids while decreasing the contacts with water. Thereafter, Artepillin C aggregates disintegrated as reflected by a decrease in the number of Artepillin C-Artepillin C contacts. From this point on, most Artepillin C molecules were in contact with DMPC instead of water, indicating that the compound was now inserted in the membrane. Nevertheless, the simulation indicated that Artepillin C molecules remained near the water/membrane interface because the contact with water remained constant in the last 200 ns even though the contact with DMPC increased.

The molecular dynamics simulations provided useful information about the interaction of Artepillin C with DMPC bilayers at the same time that they supported the experimental results discussed so far. One of the parameters, the area per lipid, increased along the MD simulation for both Artepillin C concentrations (Figure 7B)—from an initial

463 average value of 61.9 ± 1.3 Å² to 64.6 ± 1.0 Å² and 66.3 ± 1.1 Å² after 500 ns in the
464 presence of 5 and 10 Artepillin C molecules, respectively. The average membrane thickness
465 decreased slightly (by 2.2%) in the last 10 ns (Figure 7C), from 3.56 nm in pure DMPC
466 down to 3.48 ± 0.14 nm in the highly concentrated system (10 Artepillin C molceules).
467 Moreover, the presence of Artepillin C molecules induced a specific local thinning of the
468 membrane (represented by green colored areas in Figure 7C). The absolute values of
469 bilayer thickness obtained in the MD simulations were smaller than the values obtained by
470 SAXS experiments (4.64 and 4.54 nm in the absence and in the presence of Artepillin C,
471 respectively). These values agreed well, especially when one considers that the
472 experimental value represent an averaged position of the polar headgroup (z_H) and its width
473 (σ_H), whereas the theoretical value was calculated as the peak-to-peak average distance of
474 phosphate-phosphate atoms between inner and outer leaflets. Nevertheless, the same
475 relative thickness decreased by 2.2% upon addition of Artepillin C in both cases.

476 The disorder of the acyl chains, quantified by the average order parameter observed
477 during the studied thermotropic and structural alterations caused by Artepillin C in DMPC
478 model membranes, did not change significantly (Figure 7D). However, simulations with
479 five and ten Artepillin C molecules demonstrated increased mobility of the acyl chains,
480 suggesting that this feature augmented the area per lipid even when the order parameter
481 changed very little. Figure 7D shows that the major changes in order parameter occurred
482 from the 5^{th} to the 11^{th} carbon atom of the acyl chain. Curiously, the alterations in order
483 contrasted with the effects reported for other small molecules: when cholesterol, alcohol,
484 and DMSO interacted with phosphatidylcholine model membranes, an increase in area per

lipid implied an increase in the order parameter (Khajeh & Modarress, 2014; Lee et al., 2005; Vermeer, de Groot, Réat, Milon, & Czaplicki, 2007).

Figure 7E illustrates the electronic density over the last 10 ns of simulation in the presence of 10 Artepillin C molecules. Given the average phosphorous-phosphorous atom distance from the plot as compared to the above-mentioned bilayer thickness, the membrane clearly maintained its form after the Artepillin C molecules entered it. These data helped us to deduce the preferential positioning of the Artepillin C molecules. Artepillin C seemed to be equally distributed in both leaflets and resided mainly over the polar-apolar interface of the membrane, thereby influencing the regions around the lipid head group and the less profound carbon atoms of the acyl chain of the bilayer. Figure 6F depicts the equilibrium position of Artepillin C inside the bilayer during the final period of the simulation. The prenylated groups penetrated the deeper regions of the membrane, and the negative charge remained closer to the interface region, near the phosphate groups. The scheme in Figure 8 clearly shows positioning of the compound near the phosphate group as well as its orientation in the bilayer, with the carboxylic groups exposed toward water.

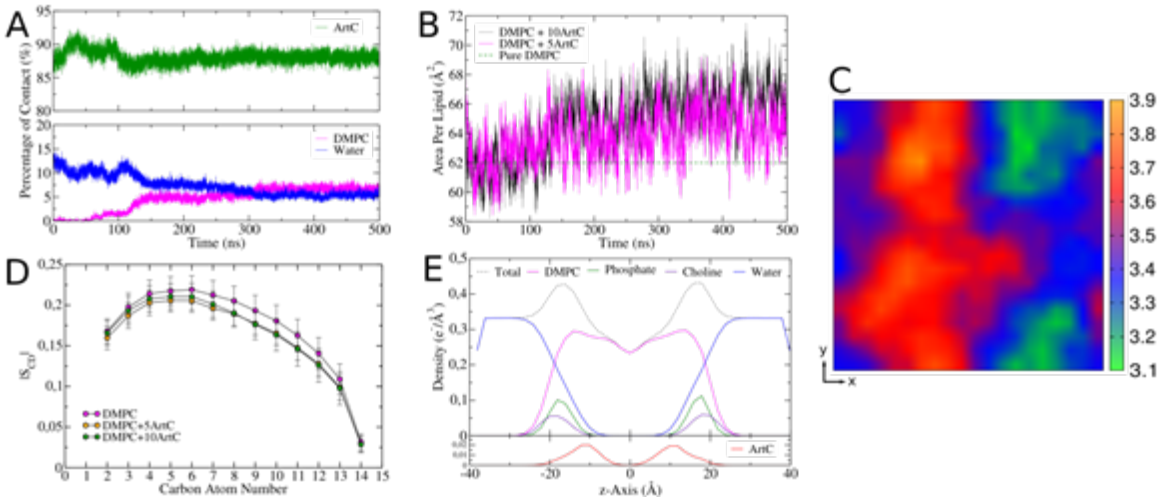

Figure. 7 A - Contact map along the 500-ns simulation; B - Area per lipid along the simulation; C - Contour map of bilayer thickness (nm) during the last 10 ns simulation (color scale represents thickness along the direction normal to the surface); D - Order parameter for the DMPC hydrophobic chains; E - Electron density profile over the last 10 ns of simulation. Two different Artepillin C/lipid molecular ratios of 5:128 and 10:128 were investigated

Molecular Dynamics simulations also provided parameters regarding the perturbation in the area per lipid in the moment Artepillin C molecules entered the lipid bilayer under constant pressure. Regardless of the amount of Artepillin C in the lipid bilayer, either 5 or 10 molecules, the area they occupied remained constant along all the simulation time, suggesting that the perturbation caused by the compound in the membrane occurred in the initial moments of its interaction with the bilayer. This result agreed with the data obtained during the Langmuir monolayer experiments, which showed that Artepillin C occupied an area of 2 $Å^2$ in the monolayer. This value corresponded approximately to the value found in the molecular dynamics simulations conducted for an Artepillin C/DMPC molecular ratio of 5:128.

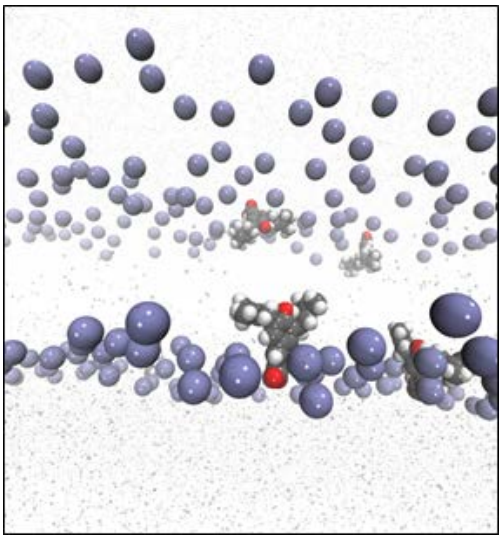

Figure. 8 Schematic illustration of the Artepillin C insertion into the lipid bilayer. The negatively charged oxygen group (red) of the carboxylic acid was oriented toward the water/lipid interface represented by the phosphate atoms (purple) and blue points (water), whereas the prenylated groups were oriented toward the hydrophobic regions

Conclusion

We have performed a series of experiments and MD simulations to understand how the main component of green propolis, Artepillin C, interacts with DMPC model membranes. In Artepillin C, the prenylated groups bound to cinnamic acid enhance the amphiphilic character of the compound and favor its insertion into the DMPC bilayer. Because the prenylated groups are relatively large, they significantly contribute to the changes promoted by Artepillin C in the vesicles. We inferred these changes from the results achieved with the use of different experimental techniques. The negativity of the electric surface potential increases due to contribution of the negative charge on Artepillin C. A higher surface pressure is necessary to disrupt DMPC monolyers containing Artepillin C. Addition of Artepillin C to DMPC increases the content of unilamellar vesicles and reduces the bilayer thickness. The presence of Artepillin C modifies the structure of the bilayer, affecting fluid lipid line defects in a way that the ripple phase and the pre-transition in the chain melting are eliminated. MD simulations detailed the interaction between Artepillin C and DMPC. Artepillin C aggregates in the aqueous phase before entering the bilayer. According to the simulations, the negatively charged group is located in the polar region of the membrane, the Artepillin C molecule is oriented in such a way that its longer symmetry axis lies along the direction normal to the surface, and heterogeneous regions emerge around Artepillin C, accompanied by a decrease in the thickness of the membrane. All this information helps to

555 understand how Artepillin C affects model membranes and contributes with knowledge
556 about the molecular mechanisms involved in the many biological actions of propolis.
557
558
559 **References**

560 Alhassan, A. M., Abdullahi, M. I., Uba, A., & Umar, A. (2014). Prenylation of Aromatic
561 Secondary Metabolites : A New Frontier for Development of Novel Drugs,
562 *13*(February), 307–314.

563 Arslan, S., Silici, S., & Percin, D. (2012). Antimicrobial activity of poplar propolis on
564 mutans streptococci and caries development in rats. *Turkish Journal of …*, *36*, 65–73.
565 http://doi.org/10.3906/biy-1101-180

566 Barioni, M. B., Ramos, A. P., Zaniquelli, M. E. D., Acuña, A. U., & Ito, A. S. (2015).
567 Miltefosine and BODIPY-labeled alkylphosphocholine with leishmanicidal activity:
568 Aggregation properties and interaction with model membranes. *Biophysical*
569 *Chemistry*, *196*, 92–99. http://doi.org/10.1016/j.bpc.2014.10.002

570 Basso, L. G. M., Rodrigues, R. Z., Naal, R. M. Z. G., & Costa-Filho, A. J. (2011). Effects
571 of the antimalarial drug primaquine on the dynamic structure of lipid model
572 membranes. *Biochimica et Biophysica Acta*, *1808*(1), 55–64.
573 http://doi.org/10.1016/j.bbamem.2010.08.009

574 Bastos, E. M. a. F., Simone, M., Jorge, D. M., Soares, A. E. E., & Spivak, M. (2008). In
575 vitro study of the antimicrobial activity of Brazilian propolis against Paenibacillus
576 larvae. *Journal of Invertebrate Pathology*, *97*(3), 273–281.

http://doi.org/10.1016/j.jip.2007.10.007

Bonvehí, J. S., & Gutiérrez, A. L. (2012). The antimicrobial effects of propolis collected in different regions in the Basque Country (Northern Spain). *World Journal of Microbiology and Biotechnology*, *28*(4), 1351–1358. http://doi.org/10.1007/s11274-011-0932-y

Fa, N., Ronkart, S., Schanck, a., Deleu, M., Gaigneaux, a., Goormaghtigh, E., & Mingeot-Leclercq, M. P. (2006). Effect of the antibiotic azithromycin on thermotropic behavior of DOPC or DPPC bilayers. *Chemistry and Physics of Lipids*, *144*(1), 108–116. http://doi.org/10.1016/j.chemphyslip.2006.08.002

Gaboriaud, F., Volinsky, R., Berman, A., & Jelinek, R. (2005). Temperature dependence of the organization and molecular interactions within phospholipid/diacetylene Langmuir films. *Journal of Colloid and Interface Science*, *287*(1), 191–197. http://doi.org/10.1016/j.jcis.2005.01.110

Gardikis, K., Hatziantoniou, S., Viras, K., Wagner, M., & Demetzos, C. (2006). A DSC and Raman spectroscopy study on the effect of PAMAM dendrimer on DPPC model lipid membranes. *International Journal of Pharmaceutics*, *318*(1–2), 118–123. http://doi.org/10.1016/j.ijpharm.2006.03.023

Gradella Villalva, D., Diociaiuti, M., Giansanti, L., Petaccia, M., Bešker, N., & Mancini, G. (2016). Molecular Packing in Langmuir Monolayers Composed of a Phosphatidylcholine and a Pyrene Lipid. *The Journal of Physical Chemistry B*, acs.jpcb.5b11836. http://doi.org/10.1021/acs.jpcb.5b11836

598 Gregoris, E., & Stevanato, R. (2010). Correlations between polyphenolic composition and
599 antioxidant activity of Venetian propolis. *Food and Chemical Toxicology*, *48*(1), 76–
600 82. http://doi.org/10.1016/j.fct.2009.09.018

601 Hamasaka, T., Kumazawa, S., Fujimoto, T., & Nakayama, T. (2004). Antioxidant activity
602 and constituents of propolis collected in various areas of Japan. *Food Science and*
603 *Technology Research Research*, *10*, 86–92.
604 http://doi.org/10.1016/j.foodchem.2006.03.045

605 Heimburg, T. (1998). Mechanical aspects of membrane thermodynamics. Estimation of the
606 mechanical properties of lipid membranes close to the chain melting transition from
607 calorimetry. *Biochimica et Biophysica Acta - Biomembranes*, *1415*(1), 147–162.
608 http://doi.org/10.1016/S0005-2736(98)00189-8

609 Heimburg, T. (2000). A model for the lipid pretransition: coupling of ripple formation with
610 the chain-melting transition. *Biophysical Journal*, *78*(3), 1154–1165.
611 http://doi.org/10.1016/S0006-3495(00)76673-2

612 Humphrey, W., Dalke, A., & Schulten, K. (1996). VMD: Visual molecular dynamics.
613 *Journal of Molecular Graphics*, *14*(1), 33–38. http://doi.org/10.1016/0263-
614 7855(96)00018-5

615 Ito, A. S., Rodrigues, A. P., Moreira Pazin, W., & Berardi Barioni, M. (2015). Fluorescence
616 depolarization analysis of thermal phase transition in DPPC and DMPG aqueous
617 dispersions. *Journal of Luminescence*, *158*, 153–159.
618 http://doi.org/10.1016/j.jlumin.2014.09.051

619 Khajeh, A., & Modarress, H. (2014). Effect of cholesterol on behavior of 5-fluorouracil (5-
620 FU) in a DMPC lipid bilayer, a molecular dynamics study. *Biophysical Chemistry*,
621 *187–188*, 43–50. http://doi.org/10.1016/j.bpc.2014.01.004

622 Kimoto, T., Arai, S., Kohguchi, M., Aga, M., Nomura, Y., Micallef, M., … Mito, K.
623 (1998). Apoptosis and suppression of tumor growth by artepillin C extracted from
624 Brazilian propolis. *Cancer Detection and Prevention*, *22*(6), 506–515.

625 Klauda, J. J. B., Venable, R. M. R., Freites, J. A., O'Connor, J. W., Tobias, D. J.,
626 Mondragon-Ramirez, C., … Pastor, R. W. (2010). Update of the CHARMM all-atom
627 additive force field for lipids: validation on six lipid types. *The Journal of Physical*
628 *Chemistry. B*, *114*(23), 7830–43. http://doi.org/10.1021/jp101759q

629 Kučerka, N., Nieh, M. P., & Katsaras, J. (2011). Fluid phase lipid areas and bilayer
630 thicknesses of commonly used phosphatidylcholines as a function of temperature.
631 *Biochimica et Biophysica Acta - Biomembranes*, *1808*(11), 2761–2771.
632 http://doi.org/10.1016/j.bbamem.2011.07.022

633 Kumazawa, S., Hamasaka, T., & Nakayama, T. (2004). Antioxidant activity of propolis of
634 various geographic origins. *Food Chemistry*, *84*(3), 329–339.
635 http://doi.org/10.1016/S0308-8146(03)00216-4

636 Laskar, R. A., Sk, I., Roy, N., & Begum, N. A. (2010). Antioxidant activity of Indian
637 propolis and its chemical constituents. *Food Chemistry*, *122*(1), 233–237.
638 http://doi.org/10.1016/j.foodchem.2010.02.068

639 Lee, B. W., Faller, R., Sum, A. K., Vattulainen, I., Patra, M., & Karttunen, M. (2005).

Structural effects of small molecules on phospholipid bilayers investigated by molecular simulations. *Fluid Phase Equilibria*, *228–229*, 135–140. http://doi.org/10.1016/j.fluid.2005.03.002

Lotfy, M. (2006). Biological activity of bee propolis in health and disease. *Asian Pacific Journal of Cancer Prevention*, *7*(1), 22–31. http://doi.org/10.1007/s00114-011-0770-7

Martínez, L., Andrade, R., Birgin, E. G., & Martínez, J. M. (2009). PACKMOL: A package for building initial configurations for molecular dynamics simulations. *Journal of Computational Chemistry*, *30*(13), 2157–2164. http://doi.org/10.1002/jcc.21224

Ota, A., Abramovič, H., Abram, V., & Poklar Ulrih, N. (2011). Interactions of p-coumaric, caffeic and ferulic acids and their styrenes with model lipid membranes. *Food Chemistry*, *125*(4), 1256–1261. http://doi.org/10.1016/j.foodchem.2010.10.054

Pabst, G., Grage, S. L., Danner-Pongratz, S., Jing, W., Ulrich, A. S., Watts, A., … Hickel, A. (2008). Membrane thickening by the antimicrobial peptide PGLa. *Biophysical Journal*, *95*(12), 5779–5788. http://doi.org/10.1529/biophysj.108.141630

Pabst, G., Koschuch, R., Pozo-Navas, B., Rappolt, M., Lohner, K., & Laggner, P. (2003). Structural analysis of weakly ordered membrane stacks. *Journal of Applied Crystallography*, *36*(6), 1378–1388. http://doi.org/10.1107/S0021889803017527

Pabst, G., Rappolt, M., Amenitsch, H., & Laggner, P. (2000). Structural information from multilamellar liposomes at full hydration: Full q -range fitting with high quality x-ray data. *Physical Review E*, *62*(3), 4000–4009. http://doi.org/10.1103/PhysRevE.62.4000

Parra, G. G., Borissevitch, G., Borissevitch, I., & Ramos, A. P. (2015). Quantum dot effects

upon the interaction between porphyrins and phospholipids in cell membrane models. *European Biophysics Journal*, 219–227. http://doi.org/10.1007/s00249-015-1088-8

Paulino, N., Abreu, S. R. L., Uto, Y., Koyama, D., Nagasawa, H., Hori, H., … Bretz, W. a. (2008). Anti-inflammatory effects of a bioavailable compound, Artepillin C, in Brazilian propolis. *European Journal of Pharmacology*, *587*(1–3), 296–301. http://doi.org/10.1016/j.ejphar.2008.02.067

Phillips, J. C., Braun, R., Wang, W., Gumbart, J., Tajkhorshid, E., Villa, E., … Schulten, K. (2005). Scalable molecular dynamics with NAMD. *Journal of Computational Chemistry*, *26*(16), 1781–802. http://doi.org/10.1002/jcc.20289

Prenner, E. J., Lewis, R. N. a H., Kondejewski, L. H., Hodges, R. S., & McElhaney, R. N. (1999). Differential scanning calorimetric study of the effect of the antimicrobial peptide gramicidin S on the thermotropic phase behavior of phosphatidylcholine, phosphatidylethanolamine and phosphatidylglycerol lipid bilayer membranes. *Biochimica et Biophysica Acta - Biomembranes*, *1417*(2), 211–223. http://doi.org/10.1016/S0005-2736(99)00004-8

Ramos, A. P., Pavani, C., Iamamoto, Y., & Zaniquelli, M. E. D. (2010). Porphyrin-phospholipid interaction and ring metallation depending on the phospholipid polar head type. *Journal of Colloid and Interface Science*, *350*(1), 148–154. http://doi.org/10.1016/j.jcis.2010.06.021

Righi, a. a., Negri, G., & Salatino, a. (2013). Comparative chemistry of propolis from eight brazilian localities. *Evidence-Based Complementary and Alternative Medicine*, *2013*. http://doi.org/10.1155/2013/267878

683 Ristori, S., Di Cola, E., Lunghi, C., Richichi, B., & Nativi, C. (2009). Structural study of
684 liposomes loaded with a GM3 lactone analogue for the targeting of tumor epitopes.
685 *Biochimica et Biophysica Acta - Biomembranes*, *1788*(12), 2518–2525.
686 http://doi.org/10.1016/j.bbamem.2009.10.005

687 Romo, T.D., Grossfield, A. (2009). LOOS: An extensible platform for the structural
688 analysis of simulations. In *31st Annual International Conference of the IEEE EMBS*
689 (pp. 2332–2335).

690 Sawaya, a C. H. F. (2009). Composition and antioxidant activity of propolis from three
691 species of Scaptotrigona stingless bees. *Journal of ApiProduct and ApiMedical*
692 *Science*, *1*(2), 37–42. http://doi.org/10.3896/IBRA.4.01.2.03

693 Shaw, D. J. (1992). *Introduction to Colloid and Surface Chemistry*. *Introduction to Colloid*
694 *and Surface Chemistry*. Elsevier. http://doi.org/10.1016/B978-0-08-050910-5.50016-5

695 Shimizu, K., Ashida, H., Matsuura, Y., & Kanazawa, K. (2004). Antioxidative
696 bioavailability of artepillin C in Brazilian propolis. *Archives of Biochemistry and*
697 *Biophysics*, *424*(2), 181–188. http://doi.org/10.1016/j.abb.2004.02.021

698 Suwalsky, M., Jemiola-Rzeminska, M., Altamirano, M., Villena, F., Dukes, N., & Strzalka,
699 K. (2015). Interactions of the antiviral and antiparkinson agent amantadine with lipid
700 membranes and human erythrocytes. *Biophysical Chemistry*, *202*, 13–20.
701 http://doi.org/10.1016/j.bpc.2015.04.002

702 Tovani, C. B., Souza, J. F. V. de, Cavallini, T. de S., Demets, G. J. F., Ito, A., Barioni, M.
703 B., … Zaniquelli, M. E. D. (2013). Comparison between cucurbiturils and β-

cyclodextrin interactions with cholesterol molecules present in Langmuir monolayers used as a biomembrane model. *Colloids and Surfaces B: Biointerfaces*, *111*, 398–406.

Vanommeslaeghe, K., Hatcher, E., Acharya, C., Kundu, S., Zhong, S., Shim, J., … Mackerell, A. D. (2010). CHARMM general force field: A force field for drug-like molecules compatible with the CHARMM all-atom additive biological force fields. *Journal of Computational Chemistry*, *31*(4), 671–690. http://doi.org/10.1002/jcc.21367

Vermeer, L. S., de Groot, B. L., Réat, V., Milon, A., & Czaplicki, J. (2007). Acyl chain order parameter profiles in phospholipid bilayers: computation from molecular dynamics simulations and comparison with 2H NMR experiments. *European Biophysics Journal : EBJ*, *36*(8), 919–31. http://doi.org/10.1007/s00249-007-0192-9

Wesołowska, O., Gąsiorowska, J., Petrus, J., Czarnik-Matusewicz, B., & Michalak, K. (2014). Interaction of prenylated chalcones and flavanones from common hop with phosphatidylcholine model membranes. *Biochimica et Biophysica Acta (BBA) - Biomembranes*, *1838*(1), 173–184. http://doi.org/10.1016/j.bbamem.2013.09.009

Yong K. Park, Severino M. Alencar, C. L. A. (2002). Botanical Origin and Chemical Composition of Brazilian Propolis. *Journal of Agricultural and Food Chemistry*, *50*, 2502–2506.

Yu, J. Q., & Matsui, Y. (1997). Effects of root exudates of cucumber (Cucumis sativus) and allelochemicals on ion uptake by cucumber seedlings. *Journal of Chemical Ecology*, *23*(3), 817–827. http://doi.org/10.1023/B:JOEC.0000006413.98507.55

Yu, W., He, X., Vanommeslaeghe, K., & MacKerell, A. D. (2012). Extension of the CHARMM General Force Field to sulfonyl-containing compounds and its utility in biomolecular simulations. *Journal of Computational Chemistry*, *33*(31), 2451–68. http://doi.org/10.1002/jcc.23067